Int. J. Electrochem. Sci., 16 **(2021)** 150927, doi: 10.20964/2021.01.63

International Journal of
ELECTROCHEMICAL
SCIENCE
www.electrochemsci.org

Effects of Alternating Current on Corrosion Behavior of X100 Pipeline Steel in Simulated Soil Solution

Yong Yang, Ming Sun, Yanlong Luo, Weiguo Zeng[*]*, Renyang He*

China Special Equipment Inspection and Research Institute, Beijing 100029, China
[*]E-mail: 39530354@qq.com

Received: 2 September 2020 / *Accepted:* 7 November 2020 / *Published:* 30 November 2020

Electrochemical measurements, immersion tests, and surface analysis technology were used to study the effects that alternating current (AC) has on the corrosion behavior of X100 pipeline steel in simulated alkaline and acidic soil solutions. In the both simulated soil solutions, the AC corrosion rates of X100 pipeline steel increased with an increase in the applied AC current density, but the increase in the rate of corrosion rates gradually decreased. The AC corrosion rate in the simulated acidic soil solution was higher than that in the simulated alkaline soil solution under the same AC current density. The direct current (DC) potential of X100 pipeline steel in the presence of AC current had a negative shift with respect to the natural potential. The real-time potential oscillated sinusoidally at the same frequency as the applied AC current, and the oscillation amplitude increased with an increase in AC current density. The AC corrosion products of X100 pipeline steel in the simulated acidic soil solution were less protective to the metal matrix than those in the simulated alkaline soil solution. For AC current densities greater than 100 A/m^2 in simulated alkaline soli solution and 200A/m^2 in simulated acidic soil solutions, localized corrosion occurred, whereas general corrosion occurred under lower AC current densities.

Keywords: X100 pipeline steel, stray AC interference, AC corrosion, corrosion behavior, simulated alkaline soil solution, simulated acidic soil solution

1. INTRODUCTION

Stray current interference can accelerate the corrosion of buried steel pipelines, but early studies [1,2] showed that corrosion caused by AC interference is less than 1% of the corrosion that is caused by the same amount of DC, and so, AC corrosion hazards to buried steel pipelines can be ignored. However, with an increasing number of oil and gas pipelines running parallel to or crossing high-voltage transmission lines or electrical railway systems, buried pipeline accidents [3-6] that are caused by AC interference in recent years have indicated that AC corrosion had become a serious hazard to buried steel pipelines. Previous studies [7-17] reported that AC corrosion generally increases with AC interference

voltage and current density and decreases with AC frequency. Uniform corrosion generally occurs under AC current density that is less than 100 A/m^2, whereas localized corrosion is likely to occur with higher AC current density. Also, the characteristics of metal and ions, oxygen content, and pH of the corrosive medium have important effects on AC corrosion. However, because of the numerous influencing factors and complex processes of AC corrosion, consensus has not yet been reached on the research conclusions.

Through the development and application of high-grade pipeline steel, the wall thickness of the steel pipe can be reduced, the weight of the steel pipe can be reduced, the welding time can be shortened, and the pipeline construction cost can be reduced [18]. Large-scale application of high-strength pipeline steel, such as X100, has become an inevitable trend in the pipeline transportation industry. Korla alkaline soil is a typical representative of saline soil in Northwest China and has good air permeability, low humidity, high salt content, and a pH of about 8.3-9.4 [19,20]. Yingtan red acidic soil is a typical acidic soil in southeastern China; it is air proof and has a high temperature, high water content, and low oxygen content with a pH of 3-5 [21]. Both types of soil are extremely corrosive to buried pipelines.

In this study, the effects of AC current on corrosion behavior of X100 pipeline steel in simulated Korla alkaline and Yingtan acidic soil solutions were studied using open circuit potential (OCP) measurements, potentiodynamic polarization, electrochemical impedance spectroscopy (EIS), scanning electron microscopy (SEM), energy dispersive X-ray spectroscopy (EDS), and weight loss tests. The purpose of this research is to provide basic technical support for stray AC interference corrosion protection of X100 pipeline steel in these typical soil environments in the future.

2. EXPERIMENTAL

2.1 Materials and solutions

The experimental material used in this study was API X100 pipeline steel, whose chemical composition and microstructure are described in detail in reference 20. Two-dimensional test specimens were prepared. Samples with dimensions of 10 mm×10 mm×5 mm were used for electrochemical testing. The back of the sample was welded with insulated copper wire, and the other surfaces (except for a working surface of 10 mm×10 mm) were sealed with epoxy resin. Samples with dimensions of 20 mm×20 mm×2 mm were used for the immersion test, and a small hole with a diameter of 2 mm was machined in one corner of the sample to connect the copper wire. The connecting copper wire was insulated with silicone, and the exposed area of the sample was about 720 mm^2. All of the working surfaces were sequentially ground to brightness without obvious scratches with waterproof emery papers that had a maximum grit of 1500, followed by cleaning in acetone, alcohol, and distilled water.

The test solutions used for this study were a simulated Korla alkaline soil solution and Yingtan acidic soil solution, whose compositions are shown in Table 1[20, 21]. The test solutions were made from analytical grade reagents and deionized water. The pH values of the solutions were adjusted by adding NaOH and acetic acid solutions.

Table 1. Chemical compositions of two kinds of simulated soil solutions (g/L)

Solutions	pH	$CaCl_2$	NaCl	Na_2SO_4	$MgSO_4·7H_2O$	$MgCl_2·6H_2O$	KNO_3	$NaHCO_3$
Korla	9.1	0.2442	3.1707	2.5276	0	0.6699	0.2156	0.1462
Yingtan	4.1	0.222	0.936	0.284	0.394	0	0.586	0.302

2.2 Electrochemical measurements

A schematic diagram of the electrochemical experimental setup, including AC interference and the electrochemical test of two electric circuits, is shown in Fig. 1. Within AC mesh, AC current supplied by the HAD-1020A digital signal generator (AC) was calculated from the measured root-mean squared (RMS) voltage drop across a 10Ω resistor (R). A 470 μF capacitor (C) was used to block possible DC current into the AC loop. A graphite electrode was used as an auxiliary electrode of the AC loop. Within the test loop, an electrochemical workstation (PARATAT 2273) was used to make electrochemical measurements under various AC current densities. A 10H inductance (L) was introduced to avoid the interference of the applied AC to the electrochemical workstation. A platinum electrode (Pt) was used as an auxiliary electrode (CE), and a saturated calomel electrode (SCE) was used as the reference electrode (RE). The electrolytic cell containing the simulated alkaline soil solution was open to the air. In contrast, the electrolytic cell used with the simulated acidic soil solution was closed, and high-purity nitrogen (99.999%) was used to purge the solution before the experiment to remove oxygen in the solution; also, the container was kept airtight during the experiment.

During the electrochemical experiment, the RMS current densities of the applied AC with a frequency of 50 Hz were 0, 30, 50, 100, 200, and 500 (300) A/m^2. Before the electrochemical experiment, the sample was cathode-polarized at -1.0V potential for 3 min to remove the oxide layer on the surface of the sample. The sample was kept in solution for half an hour, and then, the DC potential curve of the sample at various AC current densities was measured using OCP at a frequency of 1 Hz. After the DC potential was basically stable (where a maximum change in potential within 300 s did not exceed 3 mV), a potentiodynamic polarization curve measurement was conducted at a potential scanning rate of 1 mV/s under various AC current densities. The test potential was scanned from negative to positive values. A constant temperature water bath was used to control the temperature of solution during the electrochemical experiment to be 25±1℃. A high-frequency data acquisition card (ADLINK USB-1902) was used to measure the real-time potential of the sample under AC at a frequency of 5000 Hz during the immersion experiment.

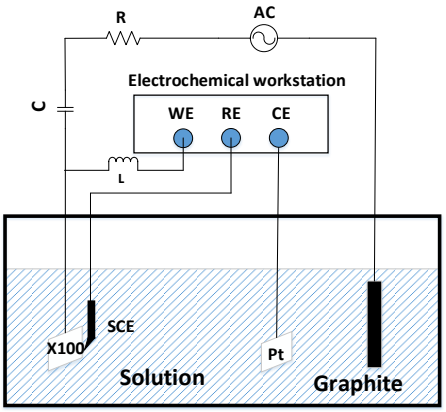

Figure 1. Schematic diagram of the experimental setup for electrochemical measurements

2.3 Immersion test

For the immersion experiment, a voltage regulator was used as an AC source; a capacitor was connected in series in the electric circuit to filter out possible DC; a rheostat was used to control the AC current density; a fixed-value resistor was connected in series to prevent a large change of the AC current density, which is caused by changes in the sample surface impedance as corrosion progressed.

During the immersion test, the RMS current densities of the superimposed AC with a frequency of 50 Hz included 0, 30, 50, 100, 200, and 500 A/m^2. An immersion test in the simulated alkaline soil solution was carried out at room temperature (about 16~26°C) for 144 h. An immersion test with the simulated acidic soil solution was carried out at room temperature (about 7-20°C) for 96 h (for corrosion rate and corrosion morphology research) and 214 h (for corrosion product research). After the tests, the weight loss sample process and the surface analysis process of the sample were the same as those in reference 21. Before and after immersion, the samples for the weight loss test were weighed using a high-precision electronic balance, and then the average corrosion rate was calculated as follows [13]:

$$R_{corr}=8.76\times \triangle W/(S\times t\times \rho) \qquad (1),$$

where ΔW is the average weight-loss of the sample in g, S is the sample exposure area in m^2, t is the soaking time in h, ρ is the density of the steel in g/cm^3, and R_{corr} is the corrosion rate in mm/a.

3. RESULTS AND DISCUSSION

3.1 Potential of samples

The time dependence of DC potentials of X100 pipeline steel in the test solutions measured at a frequency of 1 Hz under various AC current densities is shown in Fig. 2. In the alkaline soil solution,

the DC potential of the sample underwent an immediate negative shift when AC current was applied; when the AC current density was greater, the negative potential offset was greater. For example, the potential offset of the sample with a current density of 30 A/m^2 was -39 mV, whereas the potential offset of the sample with a current density of 500 A/m^2 reached -203 mV. However, when the AC current densities were greater than or equal to 50 A/m^2, the DC potential shifted from the maximum negative offset potential in a positive direction; when the AC current density was greater, the forward offset speed was faster and the offset amplitude was greater. In the acidic soil solution, the DC potential also underwent a negative shift with applied AC current, but the increase in the rate gradually decreased. For example, the potential offset was about -70 mV under an AC current density of 100 A/m^2, and the potential offset was about -98 mV under an AC current density of 300 A/m^2; however, the potential offset was only about -102 mV under an AC current density of 300 A/m^2. In contrast with the observations for the simulated alkaline soil solution, the DC potentials in the simulated acidic soil solution did not undergo positive shifting after the most negative shift with an applied AC; that is, the DC potential in the simulated acidic soil solution quickly achieved stability after the negative shift.

The results of previous theoretical studies [7, 22-27] showed that AC shifted the potential in positive or negative directions depending on the ratio of the anodic-to-cathodic Tafel slope of the electrode reaction (r). When r>1, AC shifts the corrosion potential in the positive direction; when r<1, AC current shifts the corrosion potential in the negative direction; when r=1, the corrosion potential does not change with applied AC current. When r is constant, the offset of corrosion potential increases with an increase in AC intensity and with a decrease in AC frequency. Kuang [28] reported that when the metal was not passivated, the applied AC increased the electric field strength of the electrode interface layer, thereby accelerating the diffusion rate of corrosion cations into the solution through the corrosion product layer on the metal surface and negatively shifting the potential. The positive shift in the potential under larger AC current density was because the larger current density accelerated the corrosion of steel, thickened the corrosion product layer, and retained more cations in the electric double layer; this resulted in anode concentration polarization. In the simulated acidic soil solution, corrosion products with large impedance cannot be generated, and so the potential does not undergo a positive shift under the applied AC.

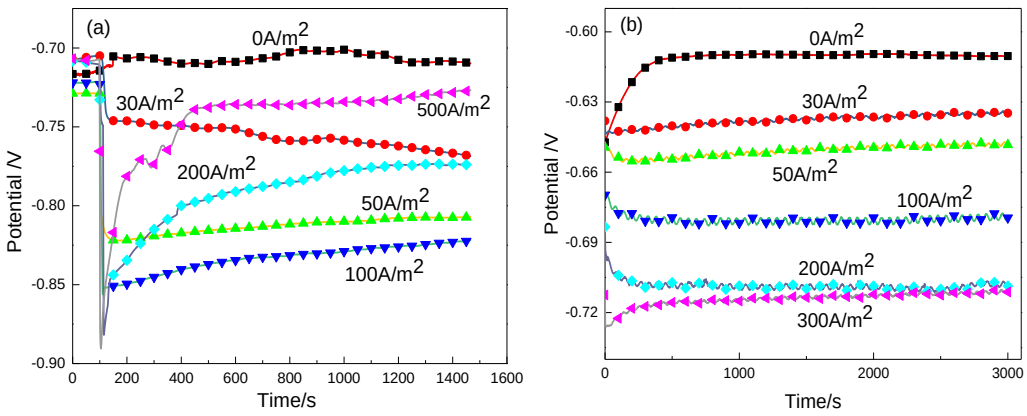

Figure 2. Time dependence of DC potential of X100 steel under various AC current densities in simulated (a) alkaline and (b) acidic soil solutions

Fig.3 shows the time dependence of the real-time potential of X100 pipeline steel in the simulated alkaline soil solution measured at a frequency of 5000 Hz under various AC current densities. The real-time potential oscillated sinusoidally with a period of 0.02 s, and the amplitude increased with an increase in AC current density. The result of sine curve fitting shows that the amplitude is 257 mV under an AC current density of 30 A/m^2, and the amplitude is as high as 2621 mV under AC current density of 500 A/m^2. It should be noted that the real-time potential in Fig.3 includes IR drop, and so the actual oscillation amplitude may be much smaller.

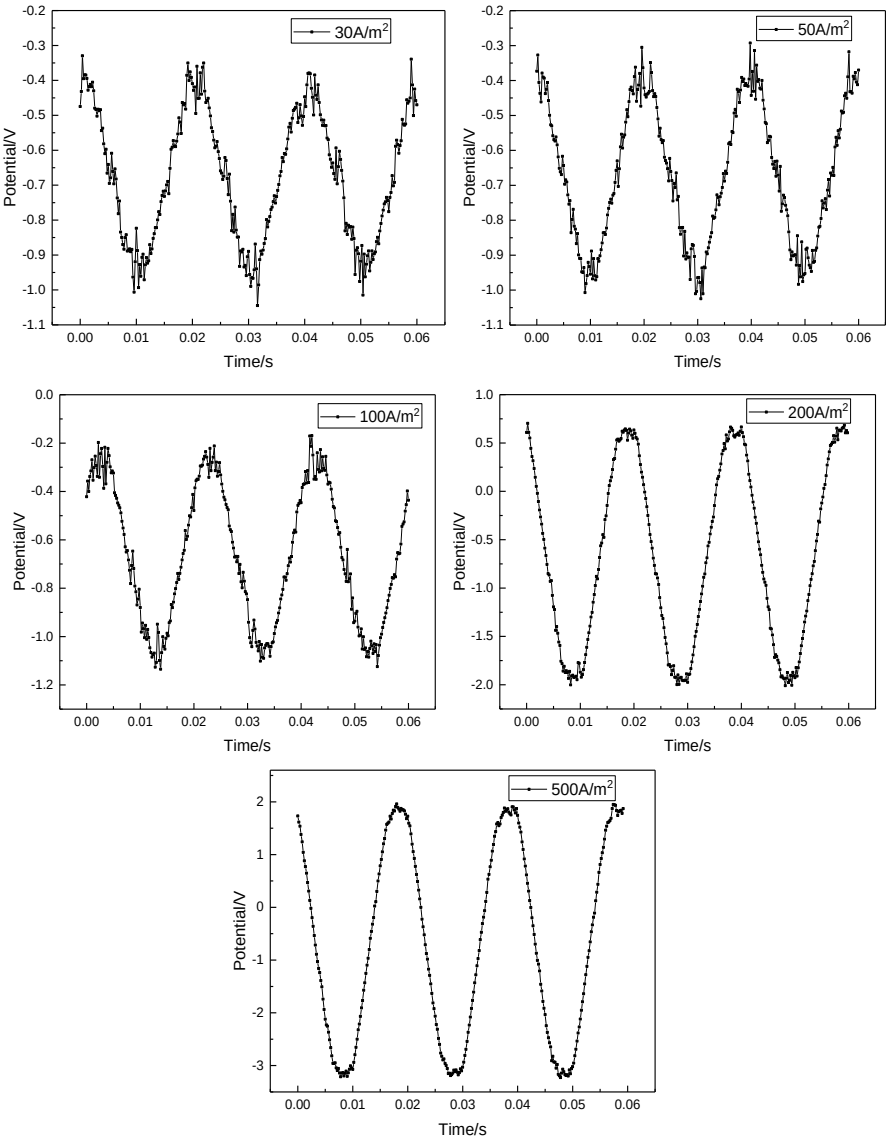

Figure 3. Real-time potential of X100 steel measured at a frequency of 5k Hz under various AC current densities in simulated alkaline soil solution

Fig.4 shows the time dependence of the real-time potential of X100 pipeline steel in the simulated acidic soil solution measured at a frequency of 5000 Hz under various AC current densities. The real-time potential in the simulated acidic soil solution was similar to that in the simulated alkaline soil solution; sinusoidal oscillations occurred at a period of 0.02 s, and the amplitude increased with an

increase in AC current density. In this experimental system, the potential oscillation amplitude was 300 mV under an AC current density of 30 A/m^2, and the potential amplitude reached 4646 mV under an AC current density of 500 A/m^2. A comparison of the potential oscillation amplitudes in the two test solutions shows that the potential oscillation amplitudes caused by the same AC current density in different corrosion systems may be different because of differences in parameters such as electrode charge transfer resistance and solution resistance.

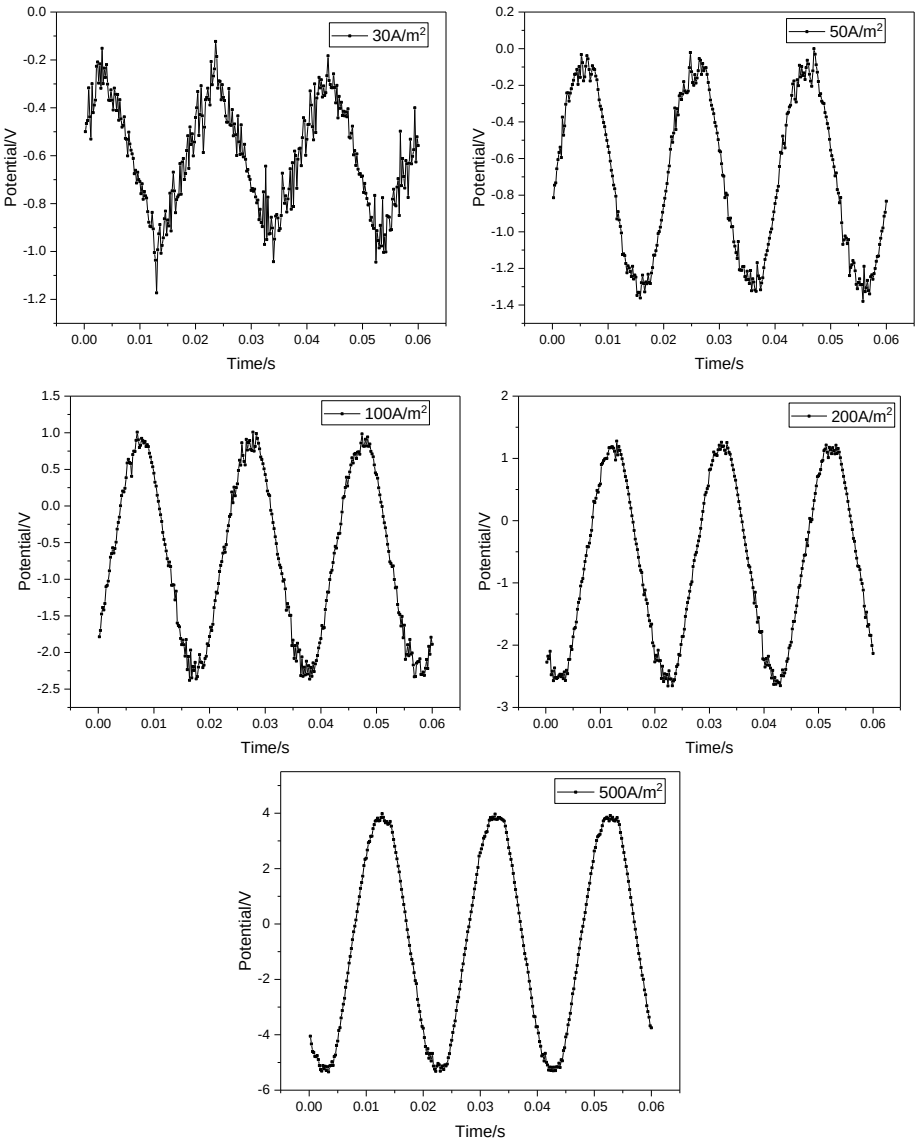

Figure 4. Real-time potential of X100 steel measured at a frequency of 5k Hz under various AC current densities in simulated acidic soil solution

3.2 Potentiodynamic polarization

Fig.5 shows potentiodynamic polarization curves of X100 pipeline steel in the simulated alkaline soil solution under various AC current densities. The X100 pipeline steel in the presence of AC was

actively dissolved. With an increase in AC current density, the trend of negative shifting with zero current potential was consistent with the results of OCP measurements. In the presence of AC interference, the cathodic polarization current, anodic polarization current, and fitted DC corrosion current density all increased. However, it is worth noting that the increase in corrosion current density was not directly proportional to the value of the applied AC current density. The influence of AC on the polarization curve of X100 pipeline steel in the simulated alkaline soil solution is similar to that of X70 and X80 pipeline steel in simulated soil solution [13].

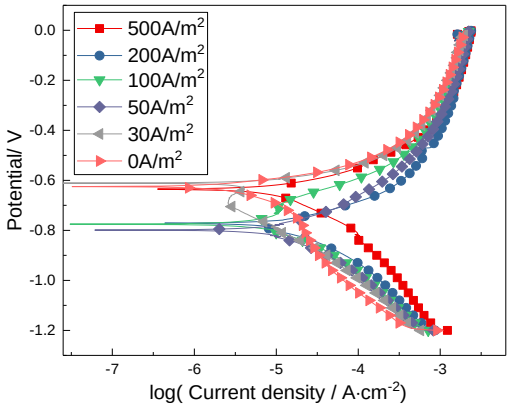

Figure 5. Potentiodynamic polarization curves of X100 steel under various AC current densities in simulated soil solution

Fig.6 shows potentiodynamic polarization curves of X100 pipeline steel in the simulated acidic soil solution under various AC current densities. And corrosion parameters obtained from the fitting of the polarization curves are shown in Table 2. The X100 pipeline steel samples in the simulated acidic soil solution under various AC current densities were also actively dissolved. The anodic polarization current decreased while the cathodic polarization current obviously increased with an increase in AC current density. In contrast to the observations of the simulated alkaline soil solution, zero current potential (E_z) underwent a positive shift with AC interference; this was the opposite of the result of OCP measurements. The slope (β_a) of the anodic polarization curve increased significantly with an increase in AC current density, for example, β_a increases from 80mV to 707mV when the AC current density increases from 0 to 300 A/m^2. The cathodic polarization process maintained diffusion control under various AC current densities. The fitted DC corrosion current density (I_{corr}) and corrosion rate (R_{corr}) calculated from I_{corr} also increased with an increase in AC current density. It can be found that R_{corr} is much smaller than corrosion rate (R_{ac}) obtained from the weight loss experiment because AC current was blocked by the inductance in the test loop.

It must be emphasized that although potentiodynamic polarization was used in some AC corrosion studies [28-33], the potentiodynamic polarization curve measured in this experiment can only be used for qualitative analysis of the corrosion process, not for accurate quantitative analysis because the inductance in the measurement loop blocked AC corrosion current.

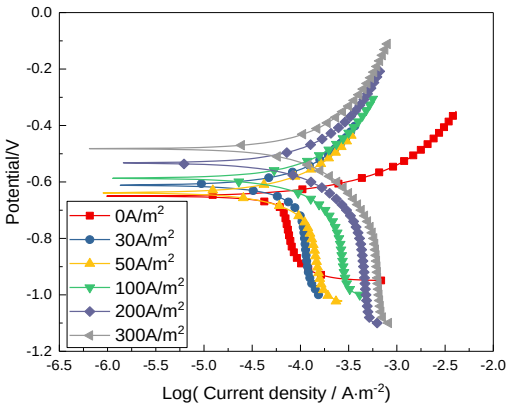

Figure 6. Potentiodynamic polarization curves of X100 steel under various AC current densities in simulated acidic soil solution

Table 2. Corrsoion parameters of X100 steel under various AC current densities in simulated acidic soil solution

I_{ac}(A/m^2)	E_z(mV)	β_a(mV/dec)	β_c(mV/dec)	I_{corr}(μA/cm^2)	R_{corr}(mm/a)
0	-654	80	1597	62.78	0.73
30	-606	321	2809	93.61	1.09
50	-636	399	1742	106.4	1.24
100	-588	504	2131	157.0	1.83
200	-534	590	3299	195.3	2.28
300	-483	707	3563	242.7	2.83

3.3 Corrosion rate

Average corrosion rates of X100 pipeline steel in the weight loss experiment in test solution under various AC current densities are shown in Fig. 7. In the two simulated soil solutions, the corrosion rates increased with an increase in AC current density. In the simulated alkaline soil solution, the corrosion rates at AC current densities of 100 A/m^2 and 500 A/m^2 were respectively about 1.7 and 2 times greater than the natural corrosion rate, which was lower than the corrosion rate of X70 and X80 pipeline steels at the same AC current density [13], and this was because of the differences of the metal and simulated solution. The corrosion rate with or without AC in the simulated acid soil solution was both higher than that in the simulated alkaline soil solution. The corrosion rates at AC current densities of 100 A/m^2 and 500 A/m^2 were respectively about 1.7 and 3 times greater than the natural corrosion rate. Although the corrosion rate with AC is obviously greater than the natural corrosion rate, it is significantly less than the theoretical corrosion rate in the case of all AC being Faraday current, as seen in Tables 3 and 4. This is believed to be because only a small part of AC participates in metal dissolution as Faraday current, and most of it is consumed in the charge and discharge of the electrode double layer [8,9,34].

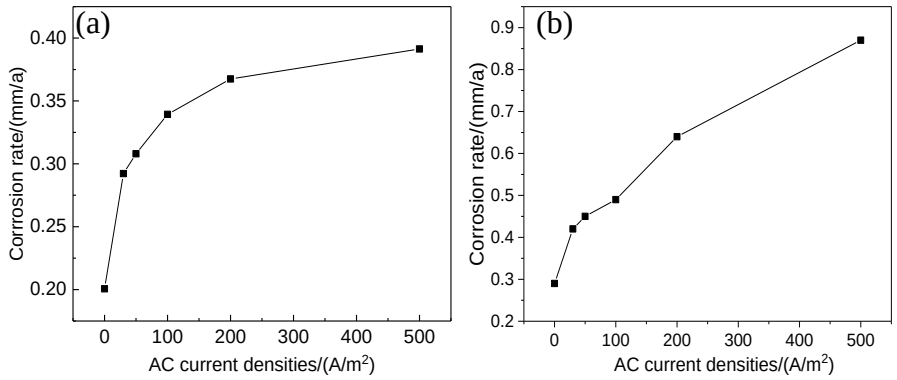

Figure 7. Corrosion rates of X100 steel under various AC current densities (a) in the simulated alkaline soil solution for 144 h and (b) in the simulated acidic soil solution for 96 h

Table 3. Comparison of corrosion rates with AC in the weight loss experiment and theoretical corrosion rates in the case of all AC being Faraday current in the simulated alkaline solution

AC densities (A/m^2)	Corrosion rates with AC in the weight loss experiment R_{ac} (mm/a)	Theoretical corrosion rates in the case of all AC being Faraday current R_t (mm/a)	R_{ac}/R_t (%)
30	0.29	34.95	0.84
50	0.31	58.24	0.53
100	0.34	116.49	0.29
200	0.37	232.98	0.16
500	0.39	582.44	0.07

Table 4. Comparison of corrosion rates with AC in the weight loss experiment and theoretical corrosion rates in the case of all AC being Faraday current in the simulated acidic solution

AC densities (A/m^2)	Corrosion rates with AC in the weight loss experiment R_{ac} (mm/a)	Theoretical corrosion rates in the case of all AC being Faraday current R_t (mm/a)	R_{ac}/R_t (%)
30	0.42	34.95	1.20
50	0.45	58.24	0.77
100	0.49	116.49	0.42
200	0.64	232.98	0.27
500	0.87	582.44	0.15

Regarding the mechanism of AC accelerated corrosion, McCollum [35] believed that AC corrosion was caused by metal ions generated in the AC anode half-cycle not being reduced in the AC cathode half-cycle. Nielsen [36] determined that the accelerated AC corrosion was a result of the combination of the alkalization of the environment near the pipeline coating holiday and the electrode interface potential oscillation caused by AC interference. Some researchers [2,8,9,27,37] reported that the cause of AC corrosion was the asymmetry of the tafel slope between the anode and cathode, which is caused by the depolarization speed of the cathode being greater than that of the anode.

3.4 Corrosion products

Fig. 8-10 show the morphology and composition analysis results of the corrosion products of X100 pipeline steel immersed in the simulated alkaline soil solution for about 144 h under various AC current densities. Macroscopically, the surface layer of the corrosion product was loose and yellow; a large amount of it fell off at the bottom of the container during the immersion process, and underneath the yellow product was a layer of a dark corrosion product. Fig. 9 shows that the corrosion products with or without AC current were composed of a loose surface layer and a relatively dense layer underneath, which had a large number of cracks. EDS analysis of the corrosion products shows that the corrosion products were mainly composed of O and Fe with small amounts of Na, S, and Cl. The compositions of elements in the surface layer and the underneath layer are similar. The amount of O in the surface layer was significantly higher than that in the underneath layer, whereas the amounts of other components in the underneath layer were higher than those in the surface layer. XRD results show that the main components of corrosion products were Fe_3O_4, FeOOH, and Fe_2O_3.

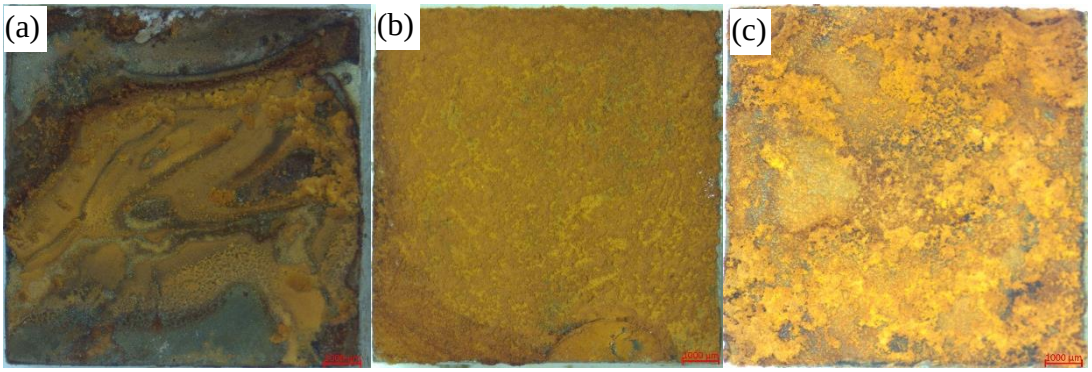

Figure 8. Optical images of corrosion products of X100 steel in the simulated alkaline soil solution for 144 h under AC current densities of (a) 0 A/m^2, (b) 50 A/m^2, and (c) 500 A/m^2

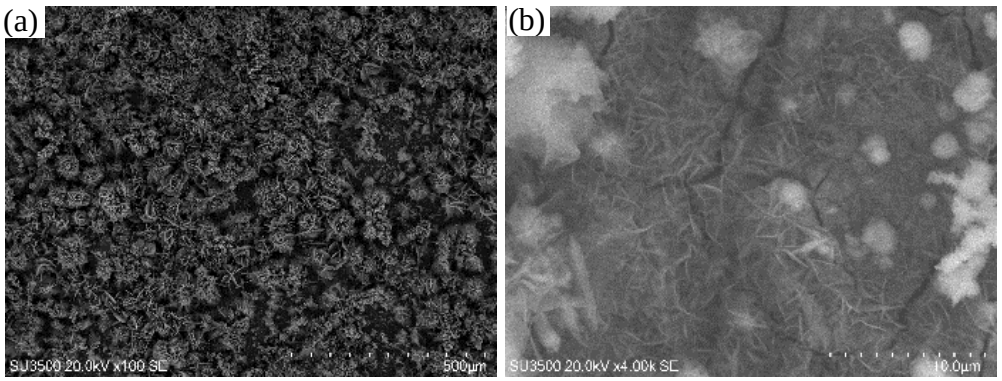

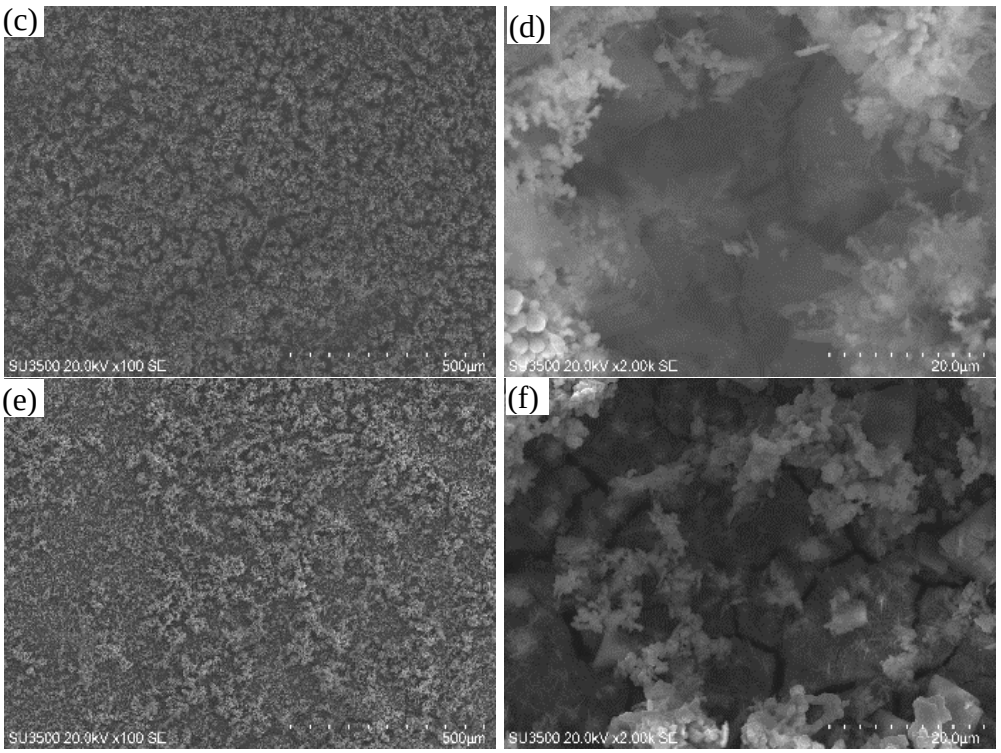

Figure 9. SEM images of the corrosion product (a, c, e) surface layer and (b, d, f) underneath layer of X100 steel after 144 h in the simulated alkaline soil solution under AC current densities of (a, b) 0 A/m^2, (c, d) 50 A/m^2, and (e, f) 500 A/m^2

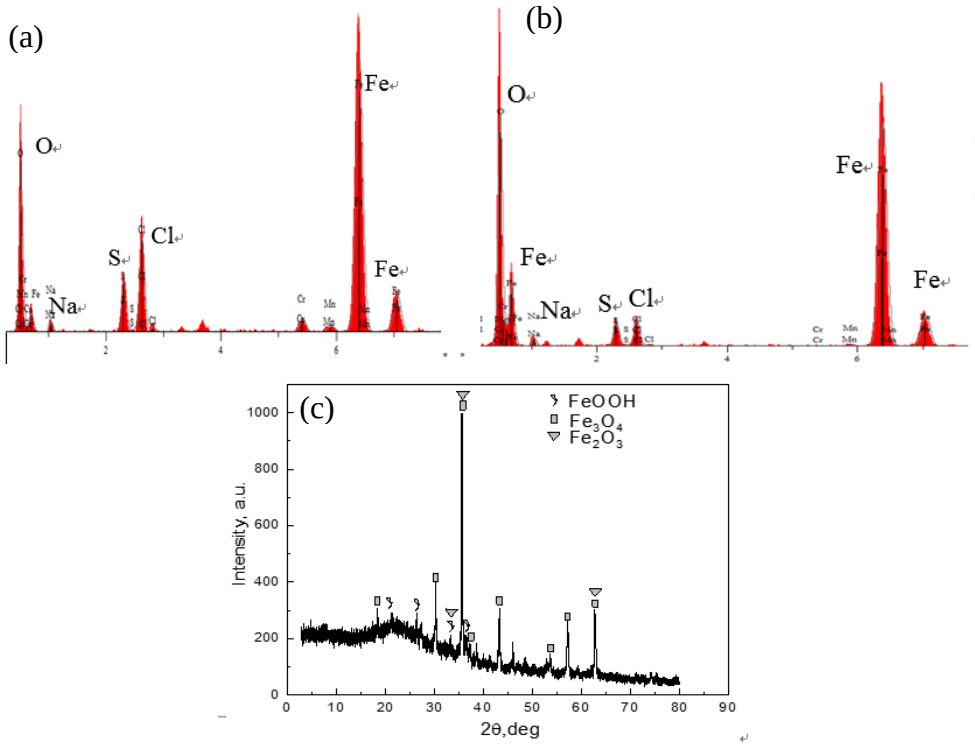

Figure 10. EDS analysis results of the corrosion product (a) surface layer and (b) underneath layer under AC current density of 50 A/m^2 and (c) XRD analysis of the corrosion product with AC current density of 500 A/m^2 immersed after 144 h in the simulated alkaline soil solution

On the basis of the components of the simulated solution and corrosion products, it is determined that the main reactions [38,39] of the corrosion process of X100 steel in the simulated alkaline soil solution are as follows:

The anode reaction mainly includes the dissolution of iron:

$$Fe \rightarrow Fe^{2+} + 2e^{-} \quad (1)$$

The cathodic reactions include:

$$2H_2O + O_2 + 4e^{-} \rightarrow 4HO^{-} \quad (2)$$

$$2H_2O + 2e^{-} \rightarrow H_2 + 2HO^{-} \quad (3)$$

The following reactions occur after Fe^{2+} diffuses from the electrode surface:

$$Fe^{2+} + 2HO^{-} \rightarrow Fe(OH)_2 \quad (4)$$

$$4Fe(OH)_2 + O_2 + 2H_2O \rightarrow 4Fe(OH)_3 \downarrow \quad (5)$$

$$Fe(OH)_3 \rightarrow FeOOH \downarrow + H_2O \quad (6)$$

$$2Fe(OH)_3 \rightarrow Fe_2O_3 \downarrow + 3H_2O \quad (7)$$

$$8FeOOH + Fe^{2+} + 2e \rightarrow 3Fe_3O_4 \downarrow + 3H_2O \quad (8)$$

$$3Fe(OH)_2 + \frac{1}{2}O_2 \rightarrow Fe_3O_4 \downarrow + 3H_2O \quad (9)$$

Because $Fe(OH)_2$ and $Fe(OH)_3$ are unstable, the final corrosion products are mainly composed of FeOOH, Fe_3O_4, and Fe_2O_3.

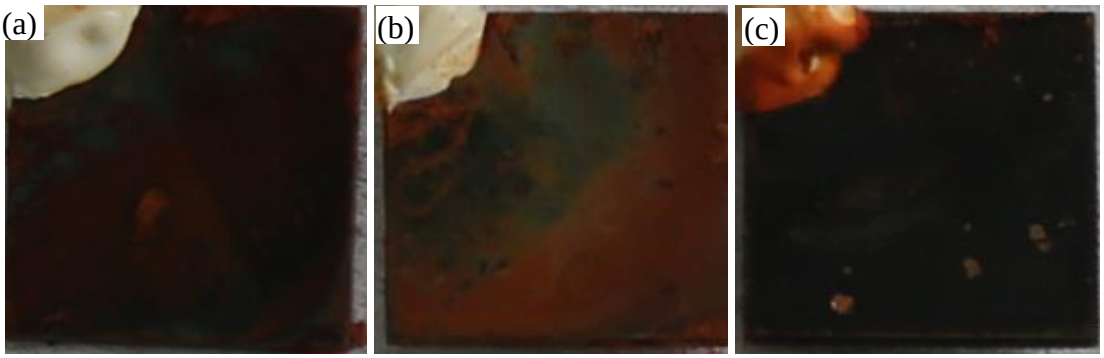

Figure 11. Optical images of the corrosion products of X100 steel in the simulated acidic soil solution after about 96h under AC current densities of (a) 0 A/m^2, (b) 50 A/m^2, and (c) 500 A/m^2

Fig. 11-13 show the morphology and composition analysis results for the corrosion products of X100 pipeline steel immersed in the simulated acidic soil solution for about 96 h under various AC current densities. Under AC current densities of 0 A/m^2 and 50 A/m^2, the corrosion products included a dense light cyan underneath layer and a small amount of a loose yellow-brown surface layer. At a current density of 500 A/m^2, a layer of black corrosion product covered the entire sample surface. The corrosion product layer that formed in the simulated acidic soil solution was relatively thin and cracked, which seemed to provide worse protection to the metal matrix than the products found in the simulated alkaline

solution. The corrosion product layers formed under various AC current densities were basically similar, and the cracks under natural corrosion conditions were relatively large. EDS analysis results show that the corrosion products that formed at various current densities were mainly composed of O and Fe, but the corrosion products that formed at a current density of 500 A/m^2 had a higher oxygen content.

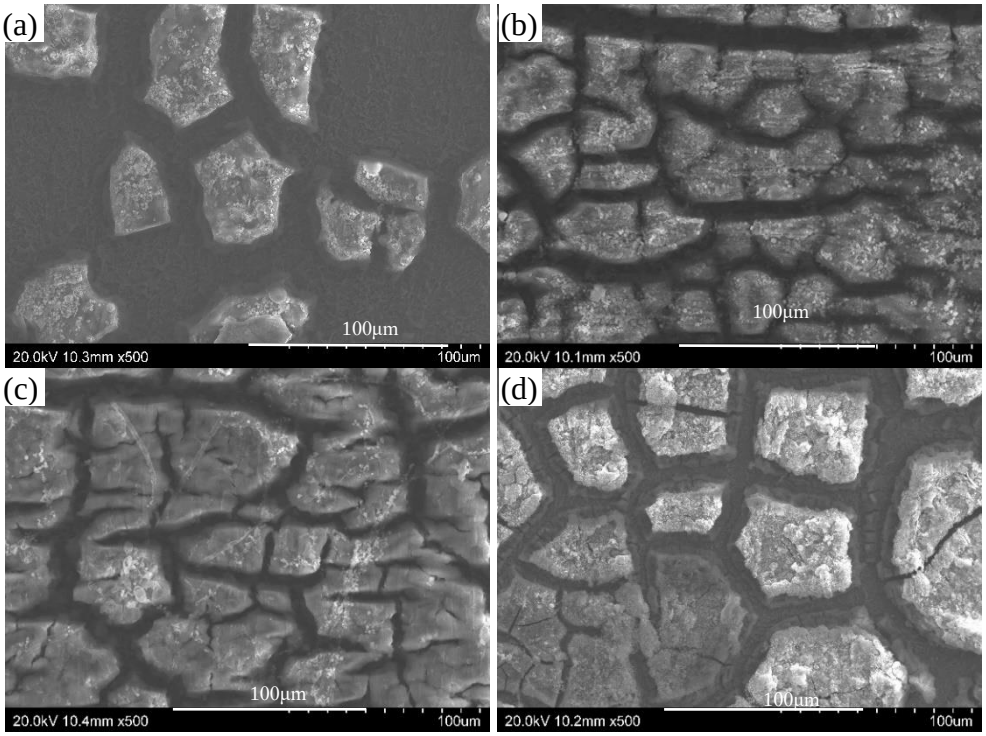

Figure 12. SEM images of corrosion products of X100 steel under AC current densities of (a) 0 A/m^2, (b) 30 A/m^2, (c) 100 A/m^2, and (d) 500 A/m^2 after 214 h in the simulated acidic soil solution

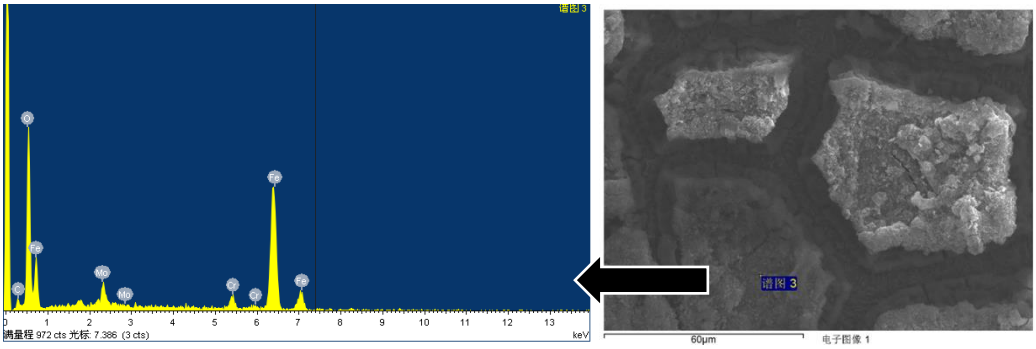

Figure 13. EDS analysis of the corrosion product of X100 steel under AC current density of 500 A/m^2 after 214 h in the simulated acidic soil solution

On the basis of the components of the simulated solution and corrosion products, it is determined that the main reactions [40] of the corrosion process of X100 in the simulated acidic soil solution are as follows:

The anode reaction mainly includes the dissolution of iron:

$$Fe-2e^- \rightarrow Fe^{2+} \quad (10)$$

The cathodic reactions include:

$$2H^+ + 2e^- \rightarrow H_2 \quad (11)$$

$$2H_2CO_3 + 2e^- \rightarrow H_2 + 2HCO_3^- \quad (12)$$

$$2H_2O + 2e^- \rightarrow H_2 + 2HO^- \quad (13)$$

The following reactions occur after Fe^{2+} diffuses from the electrode surface:

$$Fe^{2+} + 2HO^- \rightarrow Fe(OH)_2 \quad (14)$$

$$Fe(OH)_2 \rightarrow FeOOH + H^+ + e^- \quad (15)$$

Further, after FeOOH is dehydrated and reduced, corrosion products such as Fe_3O_4 and Fe_2O_3 are generated.

3.5 Corrosion morphologies

The corrosive morphologies of samples immersed in the simulated alkaline soil solution for 144 h are shown in Fig. 14. Natural corrosion was obviously uniform. Under an AC current density of 30 or 50 A/m^2, the sample still mainly underwent uniform corrosion, but many dense small corrosion pits appeared. Under an AC current density of 100 A/m^2, larger and shallower corrosion pits appeared, and the uniform corrosion characteristics were more obvious. When the current density was as high as 200 or 500 A/m^2, the sample had obvious local corrosion morphology, and when the AC current density was higher, the local corrosion was more serious. The surface corrosive morphology is consistent with the results of the weight loss experiment. Specifically, when the interference AC current density is greater, the surface corrosion is more serious.

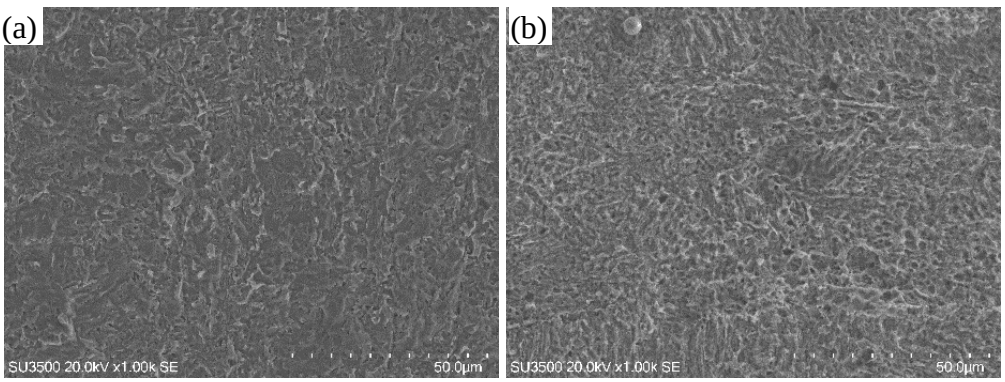

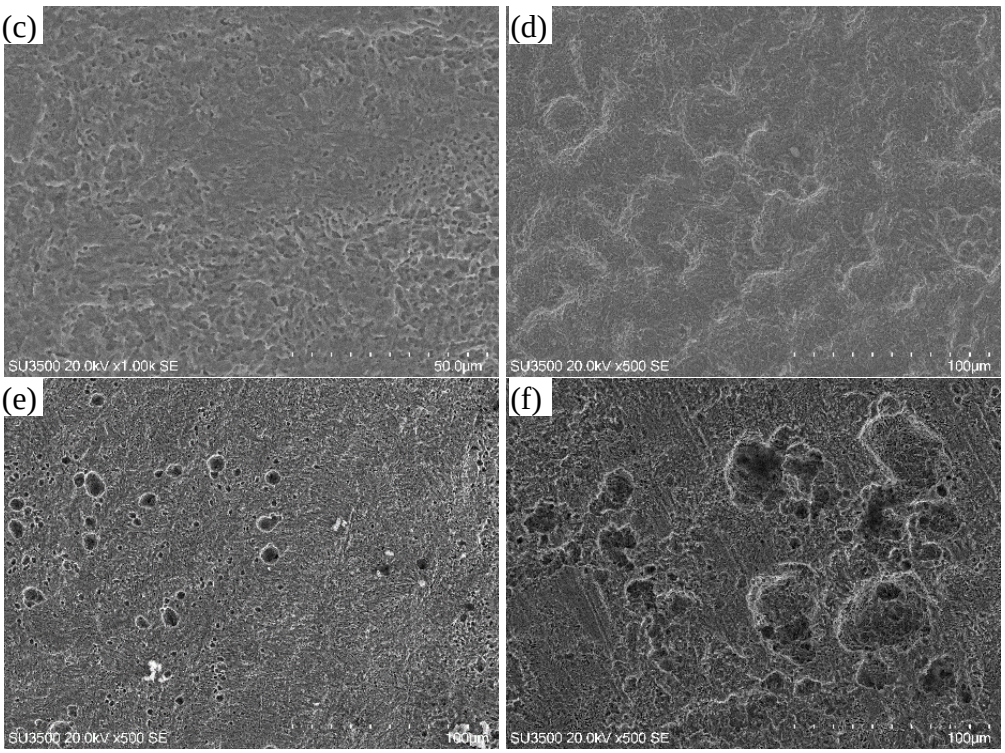

Figure 14. SEM micrographs of X100 steel in the simulated alkaline soil solution after 144 h under AC current densities of (a) 0 A/m^2, (b) 30 A/m^2, (c) 50 A/m^2, (d) 100 A/m^2, (e) 200 A/m^2, and (f) 500 A/m^2

The corrosive morphologies of the samples that were immersed in the simulated acidic soil solution for 96 h are shown in Fig. 15. In the simulated acidic soil solution, the X100 pipeline steel mainly underwent uniform corrosion in the presence of AC current, although there are some circular corrosion pits that are not larger than 10 μm on the surface of the sample under an AC current density of 500 A/m^2. Uniform corrosion without AC interference formed a very flat corrosion morphology. Uniform corrosion was obvious under AC current densities of 30 and 50 A/m^2, but the corrosion surface became rough. At an AC current density of 100 A/m^2, sporadic circular corrosion pits that were no larger than 5 μm appeared on the surface of the sample. Although there were no large local corrosion pits at an AC current density of 200 A/m^2, the surface of the sample became uneven, and this might be a result of the initial discrete small corrosion pits becoming deeper and of the pits becoming interconnected. Under an AC current density of 500 A/m^2, the surface outside the obvious circular corrosion pit is relatively flat, and this should be related to the effect of the higher polarization potential that is produced by a high AC current density.

Previous studies [28] reported that local corrosion under higher AC current density is a result of the "oscillation" effect of AC potential. The anode half-cycle of AC accelerated the corrosion and thickened the corrosion products, whereas the cathode half-cycle of AC broke the corrosion product layer, exposing the local metal to the solution and leading to corrosion in the AC current anode half-cycle. The multiple cycles of AC caused serious local corrosion. The layer of corrosion products in the simulated acidic soil solution was thinner, and there were a lot of cracks (shown in Fig.12); thus, it was

difficult to form localized corrosion.

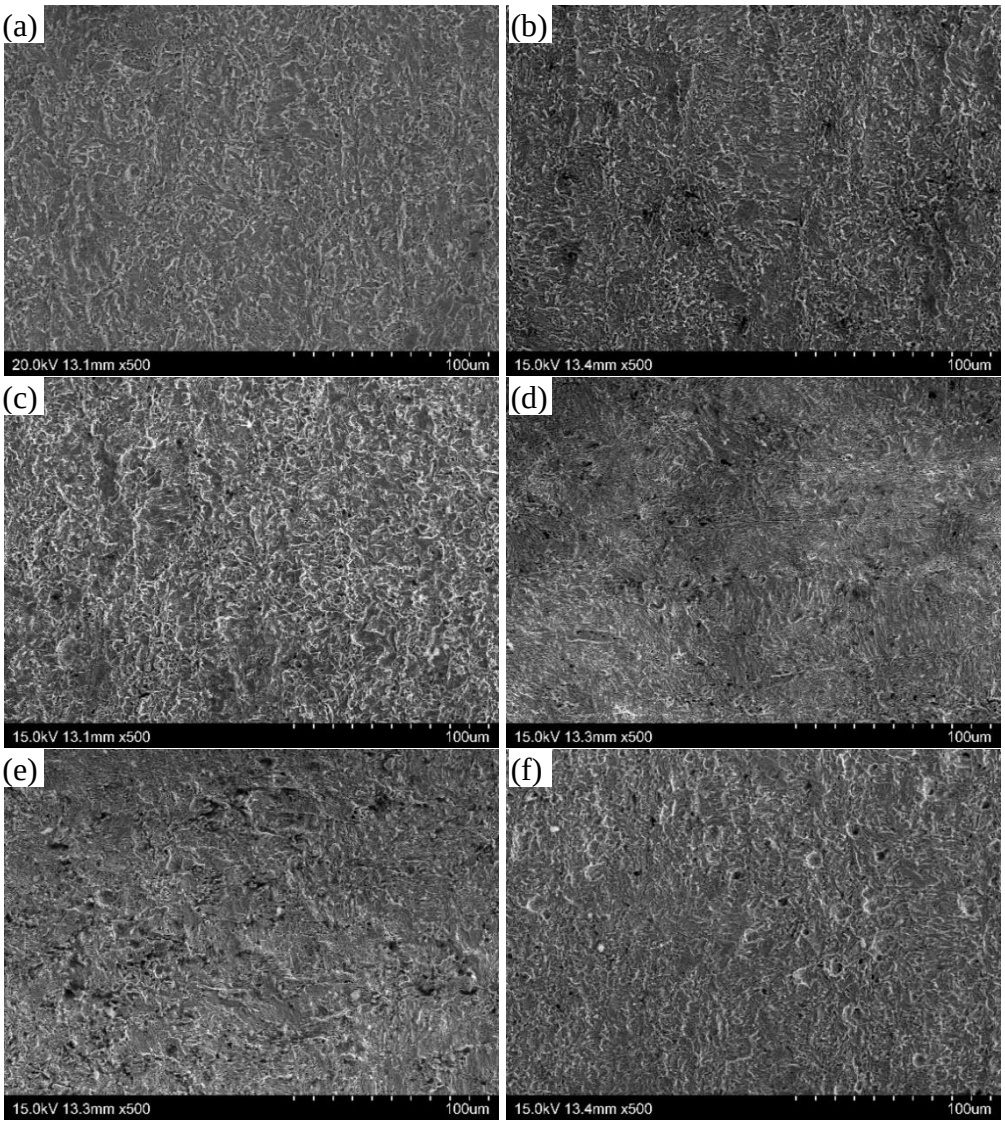

Figure 15. SEM micrographs of X100 steel in the simulated acidic soil solution after 96 h under AC current densities of (a) 0 A/m^2, (b) 30 A/m^2, (c) 50 A/m^2, (d) 100 A/m^2, (e) 200 A/m^2, and (f) 500 A/m^2

4. CONCLUSIONS

(1) In simulated alkaline and acidic soil solutions, the DC potentials immediately underwent negative shifts when AC was applied, and when the AC current density was greater, the potential shift was greater. In the simulated alkaline soil solution, an obvious positive shift occurred quickly after a DC potential negative shift when the AC current density greater than 50 A/m^2. Also, when the current density was greater, the positive offset was greater.

(2) In both of the test solutions, the AC corrosion rate of X100 pipeline steel increased with an

increase in applied AC current density, but the increase in the rate gradually decreased. Under the same AC current density, the corrosion rate in the simulated acidic soil solution was greater than that in the simulated alkaline soil solution.

(3) In both of the test solutions, the AC corrosion products of X100 pipeline steel were mainly composed of Fe and O. In the simulated alkaline soil solution, the corrosion products with or without AC interference were composed of a loose surface layer and a relatively dense underneath layer with a large number of cracks. There was only one layer of corrosion products that formed under different AC current densities in the simulated acidic soil solution, and this was relatively thin and had a large number of cracks. The corrosion products had poor protective effects on the matrix.

(4) In the test solutions, the AC current corrosive morphology of X100 pipeline steel had a similar corresponding relationship with the AC current density. Specifically, uniform corrosion occurred when the AC current density was small, and local corrosion occurred when the current density was large. In the simulated alkaline soil solution, localized corrosion occurred when the AC current density was greater than 100 A/m^2, and in the simulated acidic soil solution, localized corrosion occurred when the AC current density was greater than 200 A/m^2. Under the same current density, the local corrosion characteristics in the simulated alkaline soil solution were more obvious than those in the simulated acidic soil solution.

ACKNOWLEDGEMENTS
This research was supported by the Science and Technology Plan Projects of State Administration for Market Regulation (2019MK136), CSEI Research Program (2019-Youth-03).

References

1. F.E. Kulman, *Corrosion*, 17 (3) (1961) 34.
2. R.A. Gummow, R.G. Wakelin and S.M. Segall, ACcorrosion — a new threat to pipeline integrity? Proc.1st International Pipeline Conference (IPC), Calgary,Canada, 1996.
3. Q.Y. Fu, X.T. Wang, S.L.Chen, *Surf. Technol*., 45(02) (2016) 22.
4. A.L. Guo, J.Z. Zhen, *Oil-Gas Field Surf. Eng.g*, 37(09) (2018) 77.
5. H. R. Hanson, J. Smart, AC Corrosion on a Pipeline Located in a HVAC Utility Corridor, CORROSION/04, New Orleans, Mississipi, 2004, Paper 04209.
6. C. Movley, Pipeline corrosion from induced A.C., NACE Corrosion/2005, Houston TX, USA, 2005, Paper No. 05132.
7. S.B. Lalvani, X.A. Lin, *Corros. Sci*., 36 (1994) 1039.
8. S.B. Lalvani, G. Zhang, *Corros. Sci*., 37 (1995) 1583.
9. S.B. Lalvani, G. Zhang, *Corros. Sci*., 37 (1995) 1567.
10. S. Goidanich, L. Luciano, M. Ormellese, *Corros. Sci*., 52 (2010) 916.
11. S. Goidanich, L. Lazzari, M. Ormellese, M. Pedeferri, Influence of AC on Corrosion Kinetics for Carbon Steel, Zinc and Copper, Corrosion 2005, NACE International, Houston, 2005, Paper No. 05189.
12. X.L. Wang, M.C. Yan, Y. Shu, C. Sun, W. Ke, *J. Chin. Soc. Corros. Prot*., 37(04) (2017) 341.
13. X.H. Wang, X.T. Song, Y.C. Chen, Z.Q. Wang, L.W. Zhang, *Int. J. Electrochem. Sci.,* 13 (2018) 6436.
14. X.H. Wang, X.H. Tang, L.W. Wang, C. Wang, W.Q. Zhou, *J. Nat. Gas Sci. Eng*., 21 (2014) 474.

15. X.H. Wang, G.Y. Yang, H. Huang, Z.H. Chen, L.M. Wang, *J. Chin. Soc. Corros. Prot*., 33(4) (2013) 293.
16. H.X. Wan, D.D. Song, Z.Y. Liu, C.W. Du, X.G. Li, *Acta Metal. Sin*., 53(05) (2017) 576.
17. M. Zhu, C.W. Du, X.G. Li, Z.Y. Liu, L.Y. Wang, *J. Chin. Soc. Corros. Prot*., 34(03) (2014) 225.
18. M. Witek, *J. Nat. Gas Sci. Eng*., 27 (2015) 374.
19. P. Liang, C.W. Du, X.G. Li, *J. Chin. Soc. Corros. Prot*., 31(02) (2011) 97.
20. X.H. Wang, Y. Yang, Y.C. Chen, K.L. Wei, *Int. J. Electrochem. Sci*., 14 (2019) 9181.
21. Y. Yang, X.S. Shi, M. Sun, W.G. Zeng, *Int. J. Electrochem. Sci*., 15 (2020) 10994.
22. S.B. Lalvani, X. Lin, *Corros. Sci.,* 38 (1996) 1709.
23. R.W. Bosch, W.F. Bogaerts, *Corros. Sci*., 40 (1998) 323.
24. H.Y. Xiao, S.B. Lalvani, *J. Electrochem. Soc*., 155 (2008) C69.
25. I. Ibrahim, B. Tribollet, H, Takenouti, M. Meyer, *J. Braz. Chem. Soc.,* 26 (2015) 196.
26. I. Ibrahim, M. Meyer, H. Takenouti, B. Tribollet, *J. Braz. Chem. Soc*., 27 (2016) 605.
27. I. Ibrahim, M. Meyer, H. Takenouti, B. Tribollet, *J. Braz. Chem. Soc*., 28 (2017) 1483.
28. D. Kuang, Y.F. Cheng, *Corros. Sci*., 85 (2014) 304.
29. B.X. Wei, Q.Y. Qin, Y.L. Bai, C.K. Yu, J. Xu, *Eng. Failure Anal*., 105 (2019) 156.
30. M. Ouadah, O. Touhami, R. Ibtiouen, Z. Mourad, *IET Sci., Meas. Technol*., 11 (2017) 766.
31. Q. Liu, W. Wu, Y. Pan, Z.Y. Liu, X.C. Zhou, X.G. Li, *Constr. Build. Mater*., 171 (2018) 622.
32. Y.C. Li, C. Xu, R.H. Zhang, Q. Liu, X.H. Wang, Y.C. Chen, *Int. J. Electrochem. Sci*., 12 (2017) 1829.
33. Y.B. Guo, C. Liu, D.G. Wang, S.H. Liu, *Pet. Sci*., 12 (2015) 316.
34. L.Y. Xu, X. Su, Z.X. Yin, Y.F. Cheng, *Corros. Sci*., 61 (2012) 215.
35. B. Mccollum, G.H. Ahlborn, *Proc. Am. Inst. Electr. Eng*., 186 (1916) 301.
36. L .V. Nielsen, Role of alkalization in AC induced corrosion of pipelines and consequences hereof in relation to CP requirements [A]. Corrosion/2005 [C]. Houston, TX: NACE, 2005, paper No.05188
37. E. Ghanbari, M. Iannuzzi, R.S. Lillard, *Corrosion,* 72 (2016) 1196.
38. X.Y. Zhang, Z.Q. Shi, Y.F. Wang, *J. Chin. Soc. Corros. Prot*., 35(2015)33.
39. M.Wu, F. Xie, X. Chen，D. Wang, *J. Sichuan Univ.(Eng. Sci. Ed.),* 45(2013)185.
40. Z.Y. Liu, Z.S. Li, X.L. Zhan, W.Z. HuangFu, C.W. Du, X.G. Li, *Acta Metal. Sin*., 52 (2016) 965.